Proceedings of the 10th World Congress on Momentum, Heat and Mass Transfer (MHMT 2025)
Barcelona, Spain - April, 2025
Paper No. ENFHT 176
DOI: 10.11159/enfht25.176

Experimental Study on Heat Transfer Enhancement in Accelerated Fluid Flow through High Permeability Porous Media

Sandeep Kumar[1], Arunn Narasimhan[2]
[1,2] Department of Mechanical Engineering, IIT Madras, Chennai-600036, India
Corresponding Author: arunn@iitm.ac.in

Abstract - This experimental study investigated the heat transfer in fluid flow through rectangular channels with varying aspect ratios. Key parameters such as Nusselt number (Nu), Reynold number (Re), and total heat transfer rate (Q) were evaluated using a set of rectangular test specimens. The study analyzed how geometric configurations, including the use of a porous aluminum mesh insert, influence thermal performance and flow resistance. Two test specimens were used, each 40 mm wide and 140 mm long. The inlet height was kept constant at 40 mm, while the exit heights were changed for one of the specimens. The height of the reference specimen was fixed at 15 mm. These aspect ratio variations were used to study how different geometries affect the system's heat transfer and pressure drop. A 76 Ω nichrome wire heater was wrapped around each specimen to heat it evenly and keep a steady heat flow. This setup allowed for a controlled study of thermal performance and the effect of different aspect ratios on heat transfer. The aluminum mesh, with a wire diameter of 0.8 mm, 2770 kg/m^3 density, and a thermal conductivity of 237 W/mK, was used to improve heat transfer by increasing turbulence and surface area. The experiments were conducted across a range of Reynolds numbers from 1000 to 8000. The results show that increasing the aspect ratio improves heat transfer efficiency. With a porous medium, Aspect Ratio (AR) = 2.7 achieves a heat transfer coefficient increase ranging from 15.48% to 30.073% compared to AR = 1. Similarly, the Nusselt number for AR = 2.7 is higher by 15.48% to 23.13% than for AR = 1. These findings show that a larger aspect ratio significantly enhances heat transfer performance. Additionally, larger aspect ratios and the presence of a porous medium insert result in higher pressure gradients, with AR = 2.7 experiencing up to 3.079 times more pressure gradient than AR = 1 under the same conditions.

***Keywords*:** Heat transfer enhancement, Porous medium, Porosity, Permeability, Aspect ratio, Uniform heat flux, Pressure drop, Pressure gradient.

1. Introduction

The main objective of improving heat transfer is to handle high heat fluxes, which allows for more efficient thermal management with smaller heat exchangers, thereby reducing overall capital costs. Heat transfer enhancement techniques can be broadly categorized into active and passive methods. Active methods, like surface vibration or mechanical assistance, require external power to alter the flow pattern and improve heat transfer rates. In contrast, passive methods leverage the system's inherent energy to enhance heat transfer, often resulting in a higher fluid pressure drop. These passive techniques typically involve modifying the surface or geometry of the flow channel, such as incorporating porous inserts, to increase heat transfer efficiency.

Fluid flow and heat transfer through porous media have been extensively studied due to the potential for significant heat transfer efficiency improvements without concomitant increase in hydraulic resistance. The introduction of a porous medium in the path of a fluid's flow increases the contact surface area while simultaneously reducing the boundary layer thickness. This combination enhances convective heat transfer.

Pavel and Mohamad [1] found that using porous inserts with a diameter close to that of the pipe can significantly enhance heat transfer. In fully developed pipe flow, they observed that the Nusselt number with the porous medium insert was the highest and about 5.28 times higher than in the case without porous media. However, this improvement also resulted in the highest pressure drop of 64.8 Pa. In contrast, partially filling the pipe with porous media provided a similar increase in the Nusselt number but with a smaller rise in pressure drop compared to the fully filled pipe.

Alkam and Al-Nimr [2] studied the thermal performance of conventional heat exchangers and found that inserting porous substrates on both sides of the inner tube wall significantly enhanced performance. Their study identified the critical substrate thickness at which the improvement in thermal performance was maximum. Inserting substrates of optimal thickness resulted in the maximum performance gain with only a moderate increase in pumping cost.

Shokouhmand, Jam, and Salimpour [3] analysed the effects of placing a porous layer in the core of a channel and found

That it caused higher pressure losses compared to placing the porous medium near the walls. They concluded that when the thermal conductivity and Darcy number of the porous media are high, positioning the inserts near the walls is more effective. However, when the Darcy number is low, placing the porous layer in the channel core resulted in a higher Nusselt number.

This experimental study investigates the enhancement of heat transfer by varying the aspect ratio of a test specimen by inserting aluminum mesh porous media of high permeability 5.67×10^{-7} m^2 and porosity range (0.9 to 0.94). The aspect ratio, defined as the ratio of the longer side to the shorter side, influences the flow behavior and heat transfer mechanisms within the channel. By using different aspect ratios, the study investigates variations in boundary layer development, flow regime transitions, and heat transfer rates along the length of the specimen.

2. Experimental Procedure

This paper analyses the effect of geometry on heat transfer rates across different flow regimes (laminar, transient, and turbulent) in the presence of high-permeability porous media. A schematic of the experimental setup is shown in Figure. 1. Figure. 2 presents a photograph of the experimental setup. Figure. 3a and 3b show the test section with different aspect ratios, and Figure. 4a and 4b show the insertion of a porous medium. The setup included a double-stage reciprocating air compressor with a 500-litre storage capacity, providing a continuous supply of compressed air. The air, along with dust particles, was filtered using a filter regulator unit that removes particles of various sizes. The air dryer was equipped with a moisture separator and primary and secondary filters to eliminate moisture and dust particles up to 3 (μm. A rotameter (50-500 lpm, accuracy ±1.5) was used to measure the volume flow rate, which was precisely controlled using a ball valve.

The test section, made of mild steel, was of variable heights, ranging from H1 (40 mm) at the inlet to H2 (15 mm) at the exit. The channel width (W) was 40 mm, and the length (L) was 140 mm, remaining constant along the flow direction, which leads to a reduction in the flow section in the x-direction. A buffer length of 2.2 m and 0.5 m at the inlet and outlet ensured a fully developed flow. The experimental porous media was fabricated from a commercial aluminum screen wire with a diameter of 0.8 mm, density of 2770 kg/m^3, and thermal conductivity of 237 W/mK. The screen was cut into various sizes and mounted on steel rods. The porous screen pack was then inserted into the specimen, resulting in a porosity (ϕ) range (0.9 to 0.94). The permeability (K) was 5.67×10^{-7} m^2.

A 76 Ω nichrome resistance wire heater was used to provide a uniform heat flux, with the power adjusted by varying the voltage through a voltage regulator to control the corresponding current. A mica sheet was placed between the nichrome wire and the test section to ensure electrical insulation. To prevent heat loss to the environment, the test section was insulated

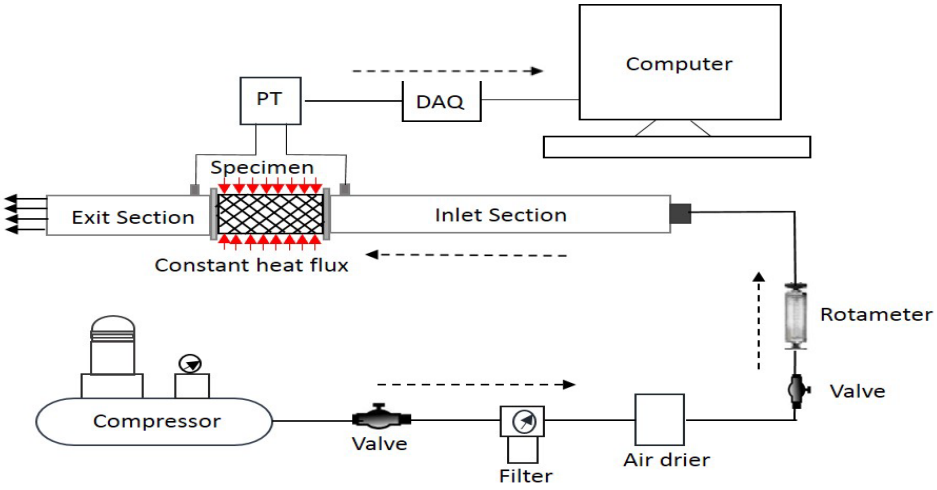

Figure.1: Schematic of experimental set-up used for Conducting experiments.

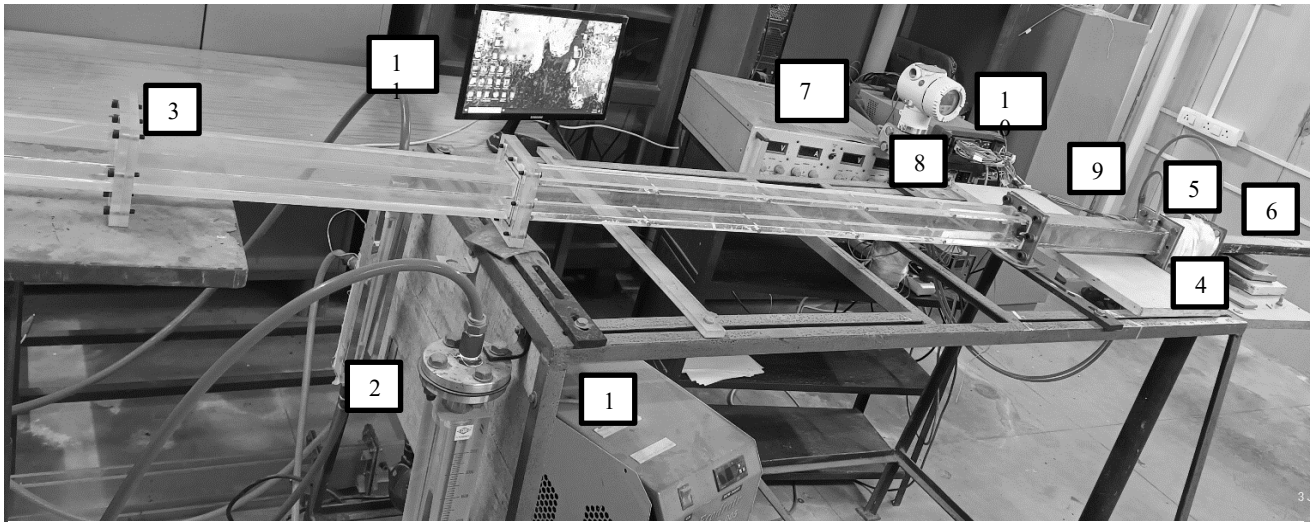

Figure 2: photograph of the experimental setup
1. Air drier 2. Rotameter 3. Inlet buffer channel 4. Test section (air flow from left to right) 5. Constant heat flux heater 6. Exit buffer channel 7 . Power supply 8. Pressure transmitter 9. Thermocouple 10. Data logger 11. PC

with a 5 mm thick ceramic wool. The air temperature was measured using K-type thermocouples (SWG 36). All thermocouples were calibrated at the Central Electronics Centre, IIT Madras, Chennai, India, using a Dry Well calibrator with PT 100, providing a 0.2°C uncertainty. The calibration range spanned from 27°C to 250°C in 5°C increments. A linear curve, derived from the calibration report, was used to compensate for thermocouple uncertainty, with an approximate uncertainty of 0.25°C.

Four thermocouples were placed on the surface to measure the wall temperature of the tube, spaced equally along the length of the test section. Another four thermocouples were positioned at the flow cross- section at the exit of the test section at radial locations to accurately measure the temperature of the heated air. A Yokogawa differential pressure transmitter, with a range of 0-1 bar and an accuracy of ±0.25%, was used to measure the pressure drop across the test section. Pressure taps were provided on each side of the test specimen for pressure measurement. All electrical signals - voltage, temperature, current, and pressure drop - were converted into digital signals by a DAQ (Data Acquisition) system connected to a PC. The experiments were conducted on all different-2 aspect ratio test specimens with various flow rate conditions but for the same power input of 12 W. A power range of 10 to 20 W is typically required for various low heating applications, such as temperature control for enclosures and electronics, cooling small batteries, and personal heating. Therefore, a 12 W power supply heater was used in this work.

Porous medium inserts of porosities ranging between 0.9 and 0.94 and permeability value 5.67×10^{-7} m^2 were placed inside all specimens. During the experiments, a constant power input was provided, and the flow rate was adjusted to achieve different Reynolds numbers. The temperature of the heated section, the air temperature, and the pressure drop were continuously monitored using an Agilent Keysight data logger connected to a PC. Initially, it took 3 to 4 hours to reach steady-state conditions, as the temperature along the surface of the specimen varied by no more than ± 0.2 ℃. Once steady-state data was collected, the flow rate was increased to obtain additional data at various flow rates under steady-state conditions. From that point onward, it took approximately 30 minutes to reach steady-state conditions for further readings, as the surface temperature remained constant for about 2 minutes after steady-state was achieved.

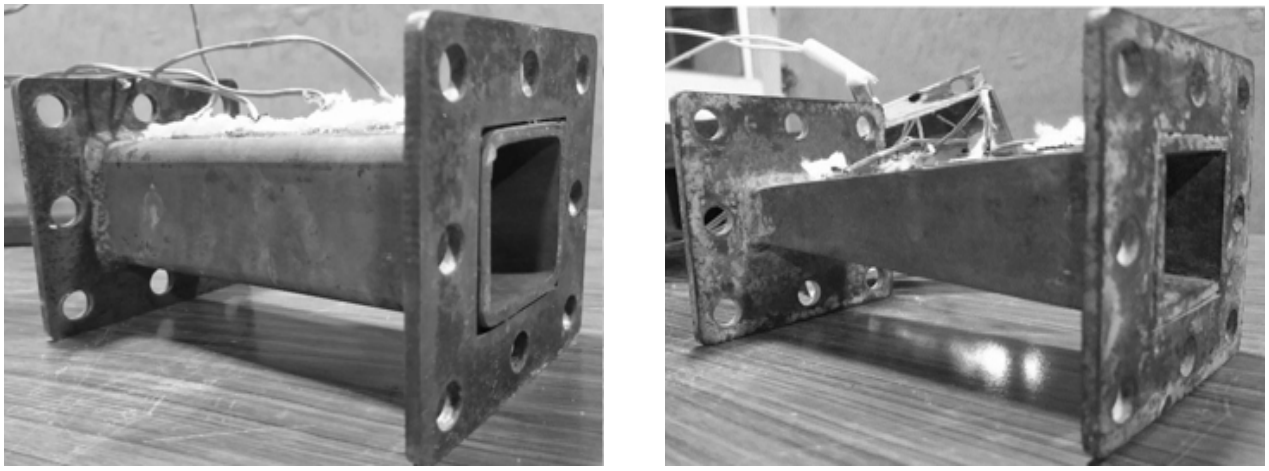

(a) Aspect Ratio = 1. b) Aspect Ratio = 2.7.

Figure 3: Various Aspect ratios specimens.

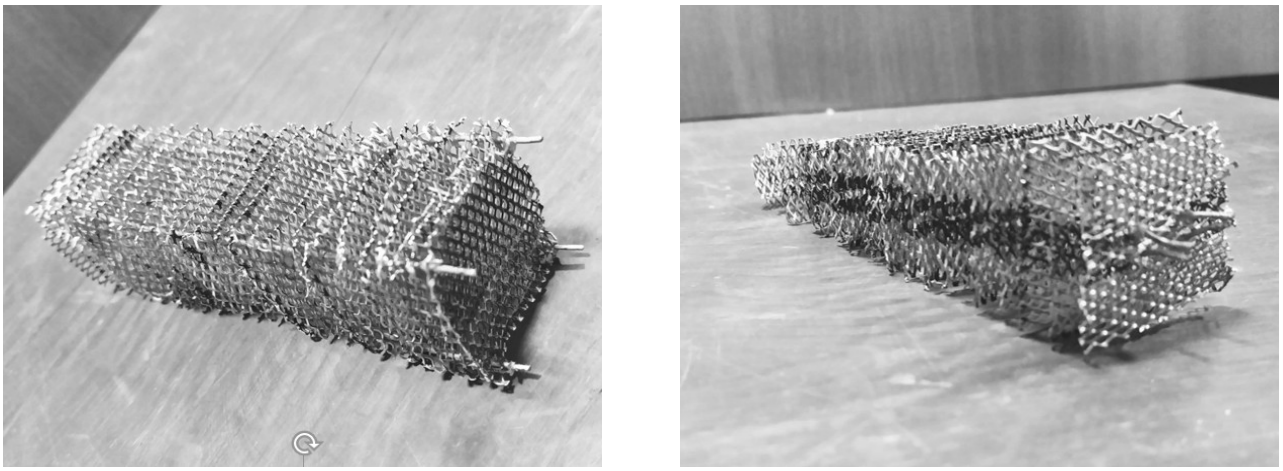

(a) Aspect Ratio = 1. b) Aspect Ratio = 2.7.

Figure 4: Various Aspect ratios porous medium.

3. Analytical Formulation

3.1 Hydrodynamic performance:

Fluid flow through porous materials is mainly influenced by three key factors porosity, permeability, and form coefficient. Porosity (ϕ) refers to the ratio of empty space to the total volume of the material, which indicates its ability to hold and transmit fluids. In this study, porosity was determined using a water displacement method. The specimen was filled with water with and without the porous material, and the difference in water volumes was a measure of the empty space in it. Porosity was then calculated as the ratio of the empty volume to the total volume of the specimen; the porosity was found to be 0.9 to 0.94 in this study.

Permeability and formation coefficients were derived from experiments measuring the pressure drop across the porous samples at different fluid inlet velocities. The relationship between the measured pressure drop per unit length and fluid inlet velocity is shown in Figure. 5. A least-squares fit was applied to this data, showing that it follows a second-order polynomial curve.

The equation for pressure drop per unit length is given as:

$$\frac{\Delta P}{L} = AU + BU^2 \tag{1}$$

The pressure drop measurements showed that the flow behavior of the porous samples analyzed in this study did not conform to Darcy's law. The quadratic term in Eq. 1 is a result of the drag force that a fluid encounters from any solid surface that obstructs its flow path. When this drag force is included in the Darcy equation, it leads to a modified version called the Hazen–Dupuit–Darcy equation, which can be expressed as [4]

$$\frac{\Delta P}{L} = \frac{\mu}{K}U + \rho C U^2 \tag{2}$$

By comparing Eq. 1 and Eq. 2, the values of K and C are determined.

$$K = \frac{\mu}{A}, \qquad C = \frac{B}{\rho}$$

Eq. 3 is the Darcy-Weisbach equation for predicting the longitudinal pressure drop across clear uniform flow is given by [4]

$$\left(\frac{\Delta P}{L}\right)_{\mathrm{CF}} = \frac{\rho}{L}(g h_{\mathrm{f}}) \tag{3}$$

The equation shows that (h_f) is the head loss in the channel, and the friction factor (f) is taken from White (2011). For laminar flow, f is calculated as 64/Re. For turbulent flow, f is found using the Colebrook equation Eq. 4 through an iterative method, based on a given Reynolds number (Re).

$$h_f = \frac{f L U^2}{2gD}\ , \left(\frac{1}{f^{1/2}}\right) = 2\log\left(0.64\mathrm{Re}_D f^{1/2}\right) - 0.8 \tag{4}$$

Eq. 5 is the Porous Medium model (PM) for predicting the global pressure drop in a uniform flow is given by [4]

$$\left(\frac{\Delta P}{L}\right)_{PM} = \frac{\mu}{K}U + \frac{\mu}{K}UX + \rho C U^2 = D_\mu + D_B + D_C \tag{5}$$

Where D_μ, D_B, and D_C represent the global viscous drag, Brinkman shear, and form drag, respectively, covering all potential drag contribution in the porous medium, including viscous drag, Brinkman shear and form drag. Eq. 6 is the Porous Medium model (PM) for predicting the global pressure drop in an accelerated flow is given by [4]

$$\begin{aligned}\left(\frac{\Delta P}{L}\right)_{\mathrm{MPM}} + \left(\frac{\Delta P}{L}\right)_{\mathrm{CF-a}} =& \frac{\mu}{K}(1+X)\left(\frac{H_1}{H_1 - H_2}\right)\ln\left(\frac{H_1}{H_2}\right)U \\ &+\rho C\left(\frac{H_1}{H_2}\right)U^2 + \frac{\rho}{L}(g h_{fa}) + \frac{\rho}{2L}(U_2^2 - U_1^2)\end{aligned} \tag{6}$$

Where MPM, X and U denote the Modified Porous Medium model (MPM model), non-dimensional Brinkman drag magnitude, and the flow velocity respectively.

3.2 Heat transfer:

The empirical Gnielinski correlation was used to compare the results of the present study with existing correlations [5]

(7)

$$Nu = \frac{\frac{f}{8}(Re - 1000)\mathrm{Pr}}{1.00 + 12.7 \cdot \sqrt{\frac{f}{8}}\left(\mathrm{Pr}^{\frac{2}{3}} - 1\right)}$$

Friction factor correlations [5]

$$f = (0.79\ln Re - 1.64)^{-2}, (2300 \leq Re_D \leq 10^4; 0.5 \leq \mathrm{Pr} \leq 200) \tag{8}$$

The power input (W) supplied to the electric heater by the power source is calculated as [6]

$$\mathrm{Q} = \mathrm{V} \times \mathrm{I} \tag{9}$$

The uniform heat flux (W/m^2) supplied by the nichrome wire heater is calculated as [3]

$$q'' = \frac{V\,I}{A_s}, \qquad \mathrm{A_s} = \mathrm{PL} \tag{10}$$

q''_{conv} = heat loss (W/m^2) from the nichrome wire heater to the environment through convection [7]

$$\mathrm{q''_{conv}} = \mathrm{q'_{loss}} = \mathrm{h_f}\left(\mathrm{T_{am}} - \mathrm{T_{loss}}\right) \tag{11}$$

where the local mean thermodynamic temperature (°C) of the air was calculated using an energy balance over an elementary control volume situated at an axial distance(x) [7]

$$T_m(x) = T_{\mathrm{in}} + \frac{q''\mathrm{A}_s}{\dot{m}c_p} \tag{12}$$

The local heat transfer coefficient, h(x), (W/m^2) is determined based on the temperature difference between the heated wall and the bulk fluid's mean temperature, given that the power dissipation at the wall is known [7]

$$h(x) = \frac{q''}{[T_s(x) - T_m(x)]} \tag{13}$$

Where n shows the number of measured local heat transfer coefficients (h), (W/m^2) the average convective heat transfer coefficient is determined as [7]

$$\overline{h} = \frac{\sum_1^{\mathrm{n}} h(x)}{\mathrm{n}} \tag{14}$$

The average Nusselt number is specified by the channel's hydraulic diameter (m). The effective thermal conductivity (W/m^2) of porous structures is calculated as the weighted geometric mean of k_f and k_S, written as [8]

$$\mathrm{Nu} = \frac{\bar{h}D}{k_{\mathrm{cff}}}, k_{\mathrm{eff}} = k_s^{(1-\phi)}k_f^{\phi} \tag{15}$$

The uncertainties in the measured values are estimated via instrument calibration or as provided by the manufacturer. The

measured physical values have errors of 0.01 millimeters for linear dimensions, ±0.2°C for temperature, and ±0.25% for pressure. The uncertainty (w_R) in the dependent variable (R) is calculated following the method indicated in [9]

$$w_R = \pm\left\{\sum_{i=1}^{n}\left[\left(\frac{\partial R}{\partial x_i}\right)^2 w_{x_i}^2\right]\right\}^{\frac{1}{2}} \tag{16}$$

Here x represents the independent variable, whereas w_x represents its uncertainty. The average Nusselt number, pressure drop, and Reynolds number have errors of ±3.56%, ±4.736%, and ±2.66%, respectively.

4. Results and Discussions

Two key factors must be considered when evaluating passive approaches to improve heat transfer in engineering applications. The first is the increased pumping power required due to system modifications, which is reflected as pressure loss. The second is the improvement in heat transfer performance, often indicated by an increase in the Nusselt number.

4.1 Hydrodynamic performance:

To validate the accuracy and reliability of the experimental setup, the obtained results were compared with the standard Porous Media (PM) model for both aspect ratios (AR = 1 and AR = 2.7), with and without porous media. Figure. 5 compares the experimental data with the PM model predictions, represented by the curves labelled Eq. 5 and Eq. 6. The percentage error between the experimental data and the PM model is 6.05% for AR=1 and 5.75% for AR=2.7.

Figure. 6 presents a comparison between the experimental data and the PM model predictions in the absence of porous media. The PM model predictions are represented by the curves labelled Eq.3 for AR=2.7 and Eq.4 for AR=1. The percentage error is 5.283% for AR=1 and 6.269% for AR=2.7, showing that the model closely matches the experimental results. The close match between the experimental results and the model predictions confirms the PM model's effectiveness in accurately capturing pressure drop behavior.

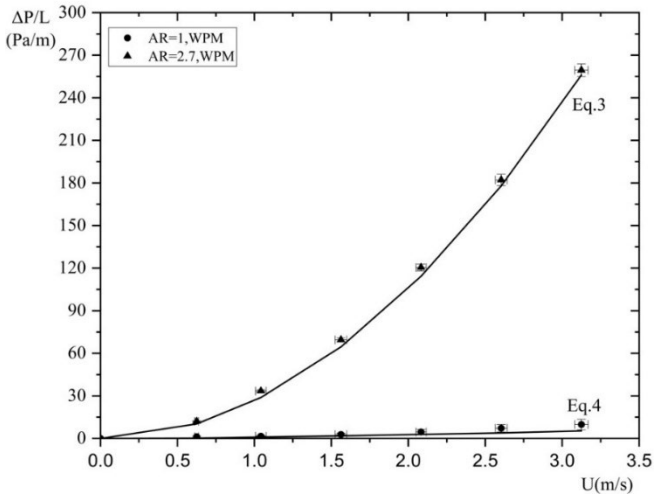

Figure 5: Validation of experimental data with analytical models for pressure gradient in porous media at different

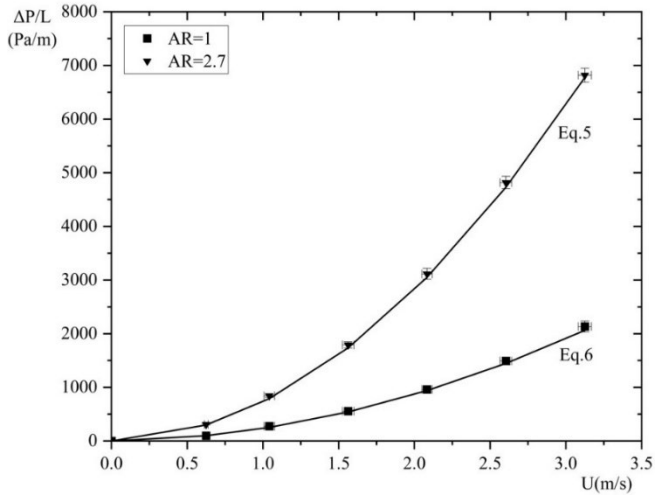

Figure 6: Variation in Pressure gradient across different aspect ratios and porous media conditions.

When comparing the two aspect ratios, the pressure gradient is higher for AR=2.7 than for AR=1 at the same flow velocity. This indicates that a larger aspect ratio increases flow resistance, likely due to changes in the geometry of the specimen. The results show that the pressure gradient for AR=2.7 is 3.079 times greater than that for AR=1. This higher pressure drop observed for AR=2.7 can be explained by increased flow resistance caused by the system's geometry. A greater

aspect ratio results in a longer and more complex flow path, increasing friction and resistance. The larger the surface area in contact with the fluid, the greater the drag, which increases the friction. The combination of a longer, more complex path and increased surface contact slows the flow, resulting in a greater pressure drop. Additionally, the non-linear terms in the Darcy-Forchheimer flow become more prominent at higher flow velocities in AR=2.7, further amplifying the pressure drop compared to AR=1.

Figure. 6 shows the 22 times increase in the pressure gradient for an aspect ratio (AR) of 2.7 compared to AR = 1, in the absence of porous media. This increase occurs because a higher aspect ratio (AR = 2.7) results in a narrower flow path, which raises the resistance to fluid movement. Physically, this means the fluid experiences more friction along the walls and greater flow disturbances.

4.2 Heat Transfer Results:

To ensure the accuracy and reliability of the experimental setup, the experimental results of the Nusselt numbers for the plain tube were compared with the values predicted by the Gnielinski correlation Eq. 7, Figure. 7 shows the experimental results alongside the predicted values. The comparison showed that the experimental Nusselt numbers deviated by only 4.19% from those predicted by the Gnielinski correlation. This close agreement between the experimental data and the standard correlation confirms the reliability and precision of both the experimental setup and the method used.

Figure. 8 shows the variation of the local heat transfer coefficient along the length of the specimen for Reynolds numbers ranging from 3000 to 8000. Four cases are examined: Porous Media with Aspect Ratio = 1, Porous Media with Aspect Ratio = 2.7, Without Porous Media with Aspect Ratio = 1, and Without Porous Media with Aspect Ratio = 2.7. The graphs display the heat transfer coefficient from the start to the end of the specimen.

An analysis of the percentage increase in the local heat transfer coefficient with Reynolds number (3000 to 8000) for different aspect ratios and porous media conditions reveals that the heat transfer coefficient is highest near the entrance and decreases along the specimen's length. As the fluid flows through the specimen, the thermal boundary layer develops. The most significant decrease in the heat transfer coefficient occurs initially, but as the flow continues, the coefficient stabilizes.

For an aspect ratio of AR = 1, the percentage increase in the heat transfer coefficient without a porous medium was 127.86%, while the inclusion of a porous medium resulted in an increase of 103.12%. For AR = 2.7, the percentage increase without a porous medium was 106.33%, while with a porous medium, it was 89.33%. Comparing the local heat transfer

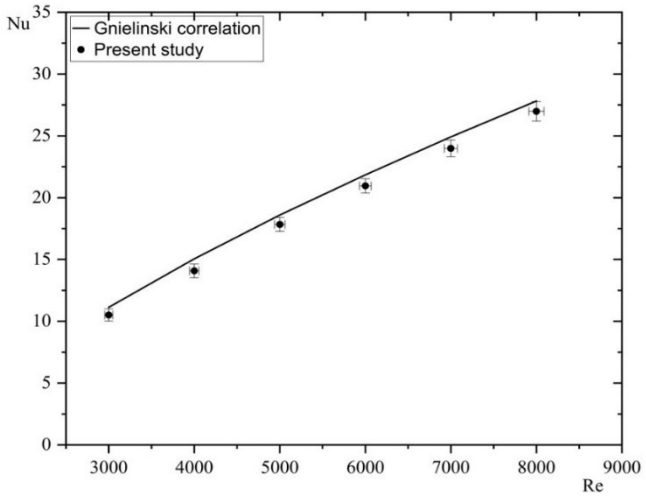

Figure 7: Comparison between experimental data and predictions from the empirical correlations for heat transfer in single-phase flow.

coefficient with and without a porous medium for the same aspect ratio (AR = 1), the percentage increase with a porous medium ranged from 110.64% to 161.24%, compared to the case without a porous medium. For AR = 2.7, the percentage increase with a porous medium ranged from 105.79% to 151.82%, in contrast to the case without a porous medium.

When comparing the two aspect ratios, AR = 1 and AR = 2.7, with a porous medium, the percentage increase in the local heat transfer coefficient for AR = 2.7 ranged from 15.48% to 30.07%, compared to AR = 1. Similarly, without a porous porous medium, the percentage increase for AR = 2.7 ranged from 17.33% to 34.43%, compared to AR = 1.

As the value of the Reynolds number increases, the value of the heat transfer coefficient also increases for all cases. This is because a higher Reynolds number indicates increased flow velocity, which enhances turbulence and mixing within the fluid. As the Reynolds number increases, the heat transfer coefficient continues to decrease along the length due to the growing boundary layer. However, at higher Reynolds numbers, the initial heat transfer coefficient is larger, indicating that turbulence and mixing in the fluid enhance heat transfer at the entrance.

The graphs show the influence of Reynolds number, aspect ratio, and porous media on the heat transfer coefficient. As the Reynolds number increases, the heat transfer coefficient also rises in both cases. However, the presence of porous media consistently results in better performance. A larger aspect ratio (AR = 2.7) further enhances heat transfer, particularly when combined with porous media, as it improves fluid flow and disrupts the boundary layer. The optimal heat transfer is observed when both a larger aspect ratio and a porous media insert are used across all Reynolds numbers.

The Nusselt number is a key parameter for evaluating convective heat transfer and enhancing it significantly improves the thermal performance of engineering systems. This study examines the impact of porous media and aspect ratios on the average Nusselt number under various conditions. The variation of the Nusselt number (Nu) with Reynolds number (Re) is shown in Figure. 9. For an aspect ratio (AR) of 1, the inclusion of a porous medium resulted in an increase in the average Nusselt number ranging from 30.47% to 67.28% compared to cases without a porous medium. In contrast, for an AR of 2.7, the percentage increase with a porous medium varied from 33.24% to 53.31% relative to the case without it. When comparing the two aspect ratios, AR = 1 and AR = 2.7 with a porous medium, the percentage increase in the average Nusselt number for AR = 2.7 ranged from 15.48% to 23.13% compared to AR = 1. Similarly, without a porous medium, the percentage increase for AR = 2.7 ranged from 13.75% to 34.35% compared to AR = 1. Thus, the combination of larger aspect ratios and porous media holds considerable potential for improving the performance of compact heat exchangers. However, it must be remembered that in real-life applications, it is essential to assess the trade-off between enhanced heat transfer and increased flow resistance.

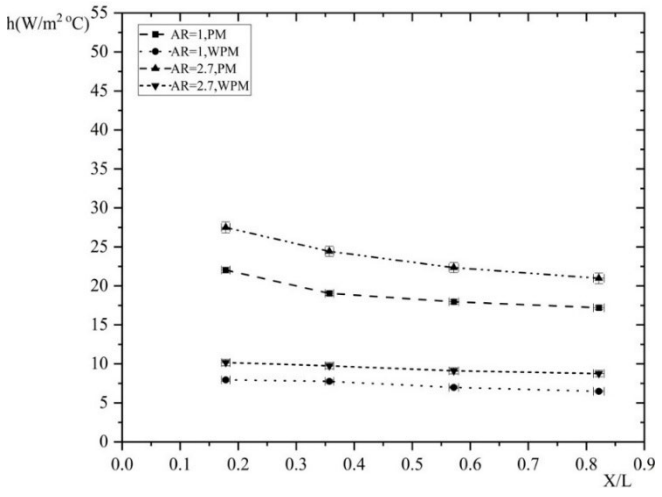

(a) Re = 3000

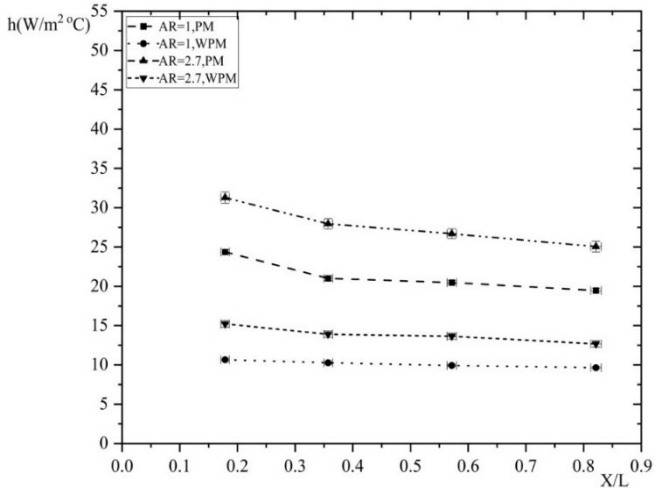

(b) Re = 4000

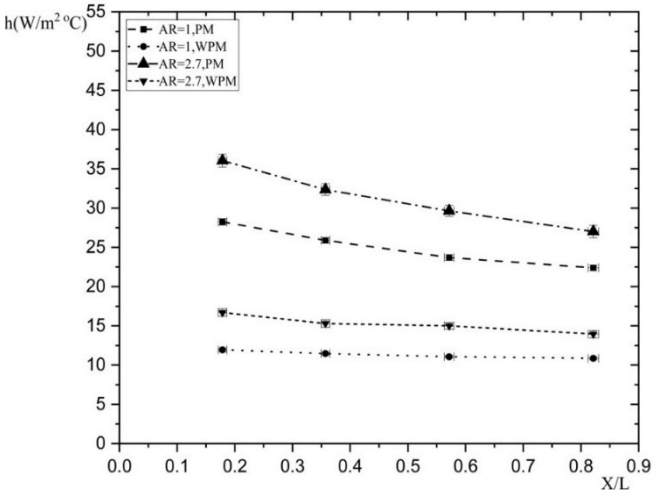

(c) Re = 5000

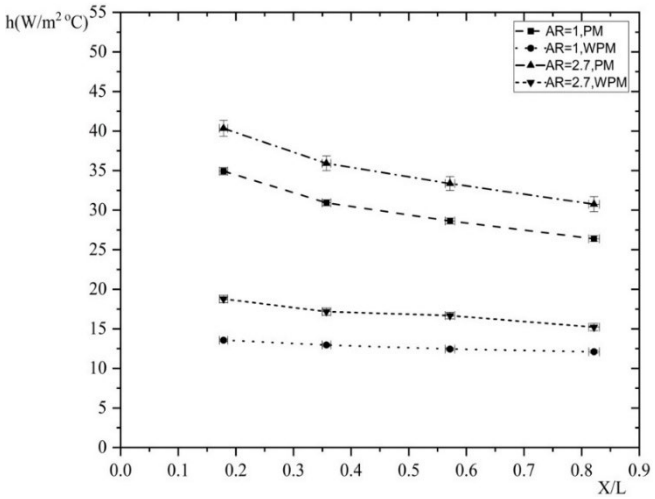

(d) Re = 6000

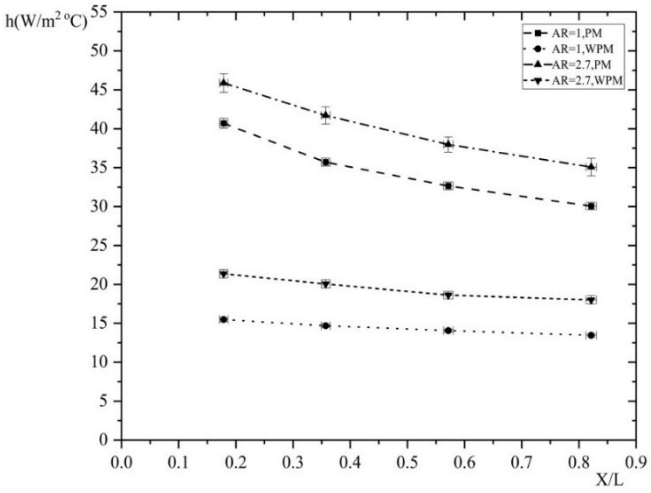

(e) Re = 7000

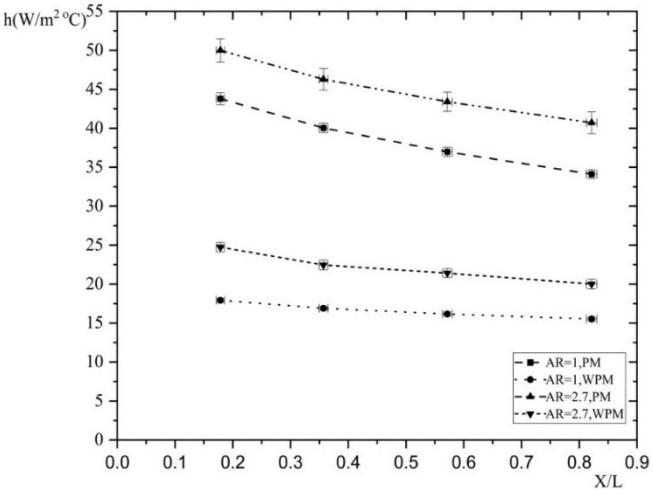

(f) Re = 8000

Figure 8: Impact of aspect ratios and porous medium on heat transfer coefficient across various flow rates.

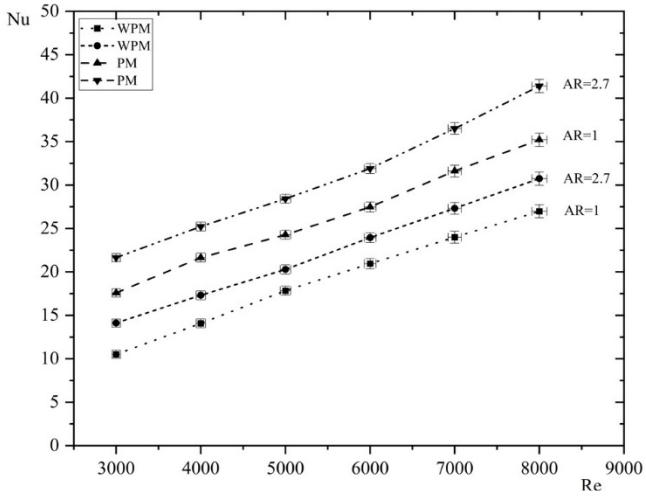

Figure 9: Comparative analysis of the effect of aspect ratio on the Nusselt number, considering cases with and without porous media.

5. Conclusion

This study investigated the effects of aspect ratios and porous medium inserts on the heat transfer characteristics of fluid flow through rectangular channels. It analysed key parameters such as the Nusselt number, Reynolds number, and heat transfer rate, considering how geometric configurations and porous media impact thermal performance and flow resistance. The experiments provide a comprehensive understanding of the relationship between aspect ratio, porous media, and heat transfer efficiency.

1) Pressure Gradient Comparison: The pressure gradient for AR = 2.7 with a porous medium was 3.079 times greater than AR = 1 under the same conditions. Similarly, in configurations without porous media, the pressure gradient for AR = 2.7 was 22.90 times that of AR = 1. This shows the significant effect of aspect ratio on flow resistance; larger aspect ratios lead to higher pressure gradients due to the impact of geometry on fluid flow dynamics.
2) Impact of Aspect Ratio and Porous medium on Nusselt: The average Nusselt number increased by 30.47% to 67.28% when a porous medium insert was present for an aspect ratio (AR) of 1. For an aspect ratio of 2.7, the increase ranged from 33.24% to 53.31% compared to scenarios without a porous medium. When comparing the two aspect ratios with a porous medium, the increase for AR = 2.7 was 15.48% to 23.13% greater than that for AR = 1. In scenarios without a porous medium, the increase for AR = 2.7 varied between 13.75% and 34.35% compared to AR = 1. Such improvements are due to better flow distribution and the disruption of the thermal boundary layer.
3) Local Heat Transfer Coefficient: The local heat transfer coefficient showed significant increases across all flow rates. The local heat transfer coefficient for AR = 1 increased from 110.243% to 161.243% with a porous medium, while for AR = 2.7, it increased from 100.17% to 151.817%. Comparing the two aspect ratios, AR = 2.7 showed a 15.48% to 30.073% increase with a porous medium and a 17.33% to 36.87% increase without it, relative to AR = 1.

The findings from this study are of use in applications that demand effective thermal management, including compact heat exchangers, electronic cooling systems, and solar energy collectors. By exploring the use of aspect ratios and porous media, the research provides valuable insights into optimizing heat transfer performance while balancing thermal efficiency and flow resistance. These results are especially beneficial for the design of systems operating in constrained spaces or those that must handle high heat flux.

References

[1] B. I. Pavel and A. A. Mohamad, "An experimental and numerical study on heat transfer enhancement for gas heat exchangers fitted with porous media," International Journal of Heat and Mass Transfer, vol. 47, no. 23, pp. 4939–4952, 2004.

[2] L. Wilson, A. Narasimhan, and S. P. Venkateshan, "Turbulent flow hydrodynamic experiments in near-compact heat exchanger models with aligned tubes," Journal of Fluids Engineering, vol. 126, pp. 990–996, 03 2005.

[3] H. Shokouhmand, F. Jam, and M. Salimpour, "The effect of porous insert position on the enhanced heat transfer in partially filled channels," International Communications in Heat and Mass Transfer, vol. 38, no. 8, pp. 1162–1167, 2011.

[4] K. Ganesan and A. Narasimhan, "Hydraulic model for accelerated flows through a porous medium in the form drag-dominated regime," Journal of Fluids Engineering, vol. 142, p. 041201, 01 2020.

[5] B. V. N. Ramakumar, J. D. Arsha, and P. Tayal, "Tapered twisted tape inserts for enhanced heat transfer," Journal of Heat Transfer, vol. 138, p. 011901, 08 2015.

6] G. K. Marri and C. Balaji, "Experimental and numerical investigations on the effect of porosity and pressure gradients of metal foams on the thermal performance of a composite phase change material heat sink," International Journal of Heat and Mass Transfer, vol. 164, p. 120454, 2021.

[7] B. I. Pavel and A. A. Mohamad, "Experimental investigation of the potential of metallic porous inserts in enhancing forced convective heat transfer," Journal of Heat Transfer, vol. 126, pp. 540–545, 04 2004.

[8] A. Narasimhan, Essentials of heat and fluid flow in porous media, vol. 61. Springer, 2013.

[9] A. ˇZukauskas, "Heat transfer from tubes in crossflow," vol. 8 of Advances in Heat Transfer, pp. 93–160, Elsevier, 1972.